Available online at www.sciencedirect.com
SCIENCE DIRECT®
Journal of the European Ceramic Society 25 (2005) 3619–3627
www.elsevier.com/locate/jeurceramsoc

Sintering and electrical conductivity in fast oxide ion conductors $La_{2-x}R_xMo_{2-y}W_yO_9$ (R: Nd, Gd, Y)

Samuel Georges[a], François Goutenoire[a], Philippe Lacorre[a,*], Marlu César Steil[b]

[a] *Laboratoire des Oxydes et Fluorures, UMR CNRS 6010, Université du Maine, Avenue Olivier Messiaen, 72085 Le Mans Cedex 9, France*
[b] *Laboratoire de Cristallochimie et de Physicochimie du Solide, UMR CNRS 8012, ENSCL, Université des Sciences et Technologies de Lille, B.P. 108, 59652 Villeneuve d'Ascq Cedex, France*

Received 6 July 2003; received in revised form 21 September 2004; accepted 24 September 2004
Available online 8 December 2004

Abstract

Attrition and ball milling are used as mechanical means to reduce grain size of optimized fast oxide-ion conductors $La_{2-x}R_xMo_{2-y}W_yO_9$ (R: rare earths). Dilatometry is used to determine the optimal sintering conditions in order to obtain high density samples (greater than 96% of relative density) with help of scanning electron microscopy to characterize their microstructure. The optimal sintering temperatures are highly dependent on the chemical composition, and therefore identical annealing temperatures do not warrant similar relative densities. Complex impedance spectroscopy show that above the transition temperature of $La_2Mo_2O_9$ at 580 °C, the conductivity of all the studied compounds is lower than that of the parent compound, whereas just below the transition, in most cases the stabilization of the cubic phase increases conductivity. An interesting result is that tungsten substitution, which stabilizes $La_2Mo_2O_9$ against reduction, does not affect significantly the oxide ion conduction.

Keywords: Milling; Sintering; Porosity; Ionic conductivity; Fuel cells; $(La, Gd)_2(Mo, W)_2O_9$

1. Introduction

Several possibilities of substitution of lanthanum or molybdenum by other iso- or aliovalent elements in the new fast oxide-ion conductor $La_2Mo_2O_9$[1] have already been reported[2–9] leading to the so-called LAMOX family. Among other applications, this type of materials could be used as solid electrolytes in some electrochemical devices such as solid oxide fuel cells (SOFCs). This application requires stringent properties to be verified. Among them figure pure fast oxide-ion conduction, thermal and electrochemical stability, and high relative density to avoid gas diffusion through the electrolyte membrane.[10]

Attempts to optimize the composition of the $La_{2-x}R_xMo_{2-y}W_yO_9$ (R: Nd, Gd, Y) series relative to both conductivity and stability against reduction were partially successful.[6–8] If molybdenum reducibility can be overcome by tungsten substitution,[8] the real effect of chemical substitution on conductivity could not be measured because of the competing effects of relative density.[7] As a matter of fact, a correlation between the pellets' density and conductivity incited us to follow a more careful approach in order to clearly identify and separate both effects. This concern, together with the necessity for an easy control and optimization of the electrolyte's relative density, is at the origin of the current study.

Attempts to improve the relative density of LAMOX materials through sintering of small particles powders have already been carried out successfully using different preparation techniques, such as for instance sol–gel,[11] freeze dried precursors[12] or impregnation of porous samples.[13] In order to avoid the problem of additional resistivity due to grain boundaries in sol–gel prepared samples, we have

* Corresponding author. Tel.: +33 2 4383 2643; fax: +33 2 4383 3506.
E-mail address: philippe.lacorre@univ-lemans.fr (P. Lacorre).

0955-2219/$ – see front matter © 2004 Elsevier Ltd. All rights reserved.
doi:10.1016/j.jeurceramsoc.2004.09.029

used attrition and ball milling to reduce the powder grain size before sintering. In this paper, we present a study on the optimization of grain size reduction and sintering conditions through dilatometry, in order to get samples of various compositions with high relative density. Their conduction properties will be studied as a function of porosity and composition.

2. Experimental

2.1. Powder synthesis

All substituted compounds were prepared by conventional solid-state reaction from a mixture of commercial powders of the elementary oxides (La_2O_3, MoO_3, Nd_2O_3, Gd_2O_3, WO_3 and Y_2O_3). Resulting from previous optimizations of properties as mentioned in the introduction, several compositions have been prepared: $La_2Mo_2O_9$, $La_{1.7}Gd_{0.3}Mo_2O_9$, $La_{1.7}Gd_{0.3}Mo_{0.8}W_{1.2}O_9$, $La_{1.4}Nd_{0.6}Mo_2O_9$ and $La_{1.9}Y_{0.1}Mo_2O_9$ as previously described.[6–8] Two of them ($La_2Mo_2O_9$ and $La_{1.4}Nd_{0.6}Mo_2O_9$) have, at room temperature, a slightly distorted monoclinic symmetry, the others being cubic.[7]

2.2. Grain size reduction

In order to reduce the mean particle size of the synthesized powders, two grinding processes were used:

- Attrition milling using a NETZCH (PE 075) molinex apparatus with small zirconia balls (2 mm diameter) into ethanol.
- Ball milling using a FRITSCH planetary micromill pulverisette apparatus equipped with agate jars and agate balls into ethanol. Note that ball milling can also be used for direct synthesis.[14]

For attrition milling the conditions were: 35 wt.% of powder in a suspension of ethanol, 1000 rpm. The morphology of the attrited powders have been characterized by scanning electron microscopy (JEOL JSM 5300), first for $La_2Mo_2O_9$, in order to determine the optimal milling time. After milling, the powder was dried for several hours into air at 80 °C and granulated with a 100 μm sieve. This method allows the treatment of a relatively large quantity of powder each time (40–50 g).

For ball milling a smaller powder quantity (typically 2–5 g) and six agate balls (around 10 mm diameter) are placed into each of the two agate jars. The milling (∼700 rpm) is realized in ethanol to reduce pollution and excessive heating during the experiment. Several tests have been carried out to determine the optimal milling time. Alternation of 15 min milling sequences with 15 min pause sequences have been applied whatever the total duration of the experiment. Indeed, in spite of the presence of ethanol, milling remains an energetic process which causes a relatively strong heating of the whole apparatus. Thus, the pause sequence allows the system to cool down between two milling sequences.

2.3. Sintering process optimization

For the dilatometric study, pellets were made from attrited powders by uniaxial pre-pressing followed by isostatic pressing at 350 MPa (diameter 5 mm and thickness ≅ 3 mm). Non-isothermal sintering behavior was investigated by dilatometric analysis (Linseis L75 dilatometer) with a heating rate of 5 °C/min up to the maximum temperature, 1 h holding time at the maximum temperature and 5 °C/min cooling rate in air. The maximum temperature was chosen as a function of the thermal stability for each compound. Relative densities of samples were determined from accurate measurements of the sample size and weight, with comparison to the theoretical density deduced from the crystal structure.

2.4. Structural characterization

The X-ray diffraction data were recorded on two apparatuses: a SIEMENS D500, and a BRUKER AXS D8 Bragg-Brentano diffractometers.

As sintered, polished and thermally etched samples were observed in a HITACHI 2300 (LE MANS) and on a JEOL JSM 5300 (LILLE) scanning electron microscope for microstructural characterization. Surfaces were previously polished with SiC paper, and grain boundaries revealed by thermal etching at 50 °C below the sintering temperature for 30 min. The energy dispersive X-ray spectra were recorded on Minipal Philips operating at 30 KeV, with a max power of 9 W.

2.5. Transport properties

For the electrical characterization, pellets (10 mm diameter and approximately 4 mm thickness) were prepared by uniaxial pre-pressing followed by isostatic pressing at 180 MPa and appropriate sintering. The electrical properties were studied by impedance spectroscopy using a Schlumberger Solartron SI 1260 frequency response analyzer with 0.1 V amplitude signal over the 32 MHz–0.1 Hz frequency range. Ten millimeter diameter pellets were used for measurements with, as electrodes, platinum deposited on both faces. The measurement's atmosphere was atmospheric air, dry air or dry nitrogen, with no influence on the measured resistances.

3. Results and discussion

3.1. Powder particle size reduction and sintering behavior

Fig. 1 shows the evolution of the powder's morphology, as a function of the attrition milling time, characterized by

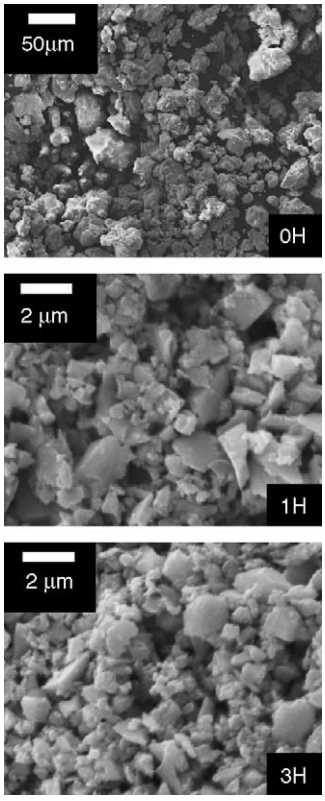

Fig. 1. SEM micrographs of $La_2Mo_2O_9$ powder for different attrition times (top: before attrition; middle: attrited for 1 h; bottom: attrited for 3 h).

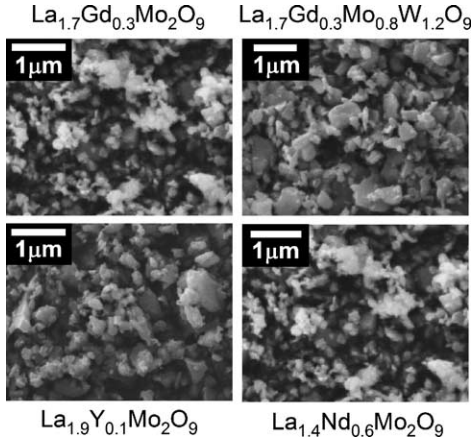

Fig. 2. SEM micrographs of LAMOX powders after attrition for 3 h.

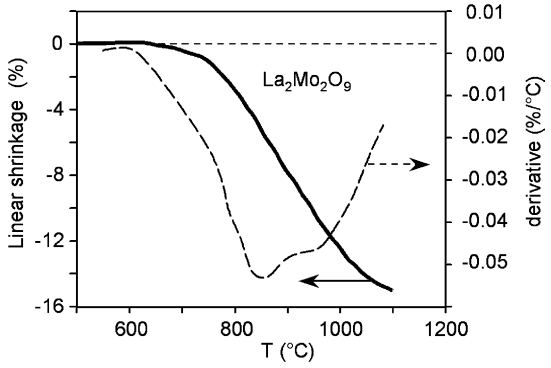

Fig. 3. Linear shrinkage and its derivative as a function of temperature for a $La_2Mo_2O_9$ pellet.

scanning electron microscopy for $La_2Mo_2O_9$. The top image has been realized on the initial powder. Particle sizes range between 10 and 50 μm, which typically corresponds to those of manually ground powders, in an agate mortar. The middle image has been taken after 1 h of attrition. The grain size is dramatically reduced during this first attrition hour since it now ranges from 0.2 to 2 μm. The bottom image has been taken after 3 h of attrition. There is no significant reduction in the grain size compared to the previous image, however, the grain size distribution is much more homogeneous. The optimal attrition time has thus been determined to be 3 h. These conditions have been applied to all the compositions described above. Fig. 2 shows that the final morphology of the powder is not composition-dependent. As a matter of fact, for the four substituted compounds, the powders present a mean particle size smaller than 1 μm.

Fig. 3 shows the dilatometric curve and its derivative for $La_2Mo_2O_9$. The shrinkage starts at approximately 700 °C and the maximum densification temperature is 850 °C. The sintering process finishes at about 1070 °C with a final shrinkage of approximately 16%. This material behaves as many other ceramics: the first essential step is a densification process by porosity elimination, the second being a grain growth step. In order to optimize the sintering conditions for $La_2Mo_2O_9$ powder, two temperature points were selected from the shrinkage curves (near the maximal shrinkage domain): 1000 and 1050 °C, 1 h holding time being applied at 1000 °C, and 1, 2 and 10 h holding times at 1050 °C. Heating and cooling rates were 5 K min^{-1}. Table 1 shows the relative densities of ceramic samples for different sintering temperatures and times. For all samples, the relative densities are higher than 95%. The samples sintered at 1050 °C reach the maximum relative density values (around 97%) for all sintering times. The relative densities in Table 1 were determined by mass and size measurements. These results were confirmed using He picnometry, a more accurate method. Indeed, during the sintering process, pellets are often deformed and may show leading cracks, which lead to inaccuracies of the dimension measurements. Specimens sintered at 1000 °C/1 h and 1050 °C/2 h reach a relative density value of 96.8 and 98.0, respectively. These results were corroborated by SEM micrographs (Fig. 4) obtained for $La_2Mo_2O_9$

Table 1
Relative densities as a function of sintering temperature in $La_2Mo_2O_9$[a]

Sintering temperature (°C)	Sintering time (h)	Relative density (%)[a]
1000	1	95.7 ± 0.5
1050	1	97.0 ± 0.5
1050	2	97.2 ± 0.4
1050	10	97.3 ± 0.4

[a] Theoretical density = 5.576 g cm^{-3}.

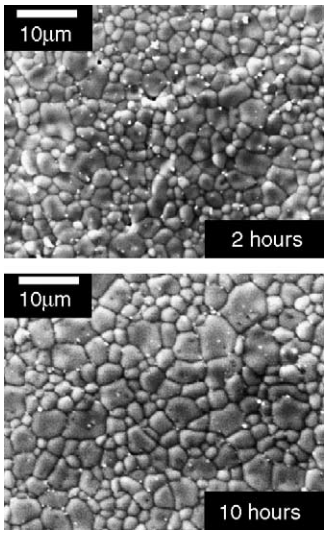

Fig. 4. SEM micrographs of the surface of $La_2Mo_2O_9$ sintered pellets, after a thermal plateau at 1070 °C for 2 h (top) and 10 h (bottom).

pellets sintered at 1050 °C after a 2 h plateau (top), and a 10 h plateau (bottom). The microstructure of the pellets is fully dense. An increase of the grain size with increasing sintering time is noticed, which confirms the nature of the second essential step detected by non-isothermal sintering (Fig. 3). In both cases, the pictures only show a small quantity of closed porosity.

On the basis of this study, the sintering conditions were determined for the four substituted compounds. The influence of the cation substitution on the densification behavior of LAMOX materials can be clearly observed in Fig. 5. This figure evidences that the sintering is strongly dependant on the chemical composition. In the same conditions, the shrinkage begins around 650 °C for $La_{1.4}Nd_{0.6}Mo_2O_9$, and around 800 °C for $La_{1.7}Gd_{0.3}Mo_{0.8}W_{1.2}O_9$, and is complete at around $T = 950$ and 1150 °C, respectively. This effect is not related to the initial particle size, since it is similar for both compositions (Fig. 2). Lanthanum site substitutions decrease the sintering temperature, while molybdenum site substitution increases it. Thus, we have determined the

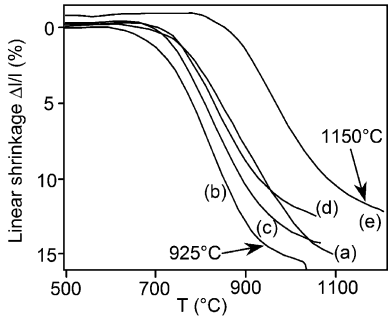

Fig. 5. Linear shrinkage as a function of temperature of LAMOX pellets issued from attrited powders: (a) $La_2Mo_2O_9$; (b) $La_{1.4}Nd_{0.6}Mo_2O_9$; (c) $La_{1.9}Y_{0.1}Mo_2O_9$; (d) $La_{1.7}Gd_{0.3}Mo_2O_9$; (e) $La_{1.7}Gd_{0.3}Mo_{0.8}W_{1.2}O_9$.

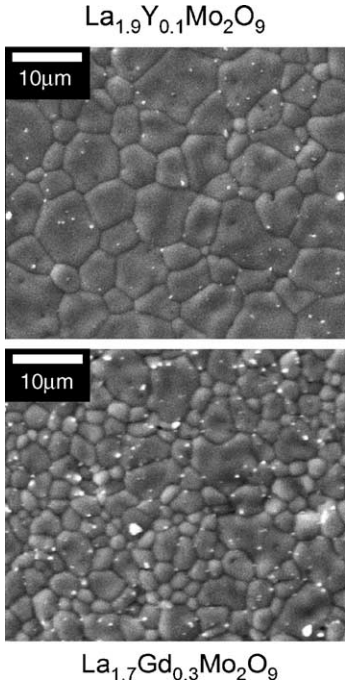

Fig. 6. SEM micrographs of sintered LAMOX pellets $La_{1.9}Y_{0.1}Mo_2O_9$ and $La_{1.7}Gd_{0.3}Mo_2O_9$. Refer to the text for the sintering conditions.

sintering temperatures for all the compositions: 1050 °C for $La_2Mo_2O_9$, 925 °C for $La_{1.4}Nd_{0.6}Mo_2O_9$, 1000 °C for $La_{1.7}Gd_{0.3}Mo_2O_9$ and $La_{1.9}Y_{0.1}Mo_2O_9$, and 1150 °C for $La_{1.7}Gd_{0.3}Mo_{0.8}W_{1.2}O_9$ during 2 h. In all cases, the reached relative density is around 96%, with a small quantity of closed porosity, but the average grain size is slightly different depending on composition (see Fig. 6 for examples of face-unpolished pellets). It varies from 2 to 5 µm for $La_2Mo_2O_9$ and $La_{1.7}Gd_{0.3}Mo_2O_9$, and 2 to 10 µm for $La_{1.9}Y_{0.1}Mo_2O_9$. This small difference indicates that the grain growing step, in our conditions, begins first for $La_{1.9}Y_{0.1}Mo_2O_9$ and $La_{1.4}Nd_{0.6}Mo_2O_9$. Fig. 5 also evidences the melting of $La_{1.4}Nd_{0.6}Mo_2O_9$ at 1030 °C, while $La_{1.7}Gd_{0.3}Mo_{0.8}W_{1.2}O_9$ is still solid above 1200 °C. The sintering and melting temperatures are clearly related.

This sintering conditions determination allowed us to prepare dense samples for physical properties characterization. The large sintering temperature ranges could be an advantage considering thermo-mechanical compatibility with electrode materials. Indeed, the possible co-sintering conditions between a LAMOX-type electrolyte and an electrode material could consequently be very wide and modulated through chemical composition, especially tungsten content. LAMOX ceramics are creamy colored and mechanically stable. Only the $La_2Mo_2O_9$ parent compound's pellets sometimes break while cooling. The phase transition occurring at 580 °C from the cubic to the monoclinic phase[2] is responsible for an abrupt change of the cell volume, which introduces strong constraints in a dense sample.

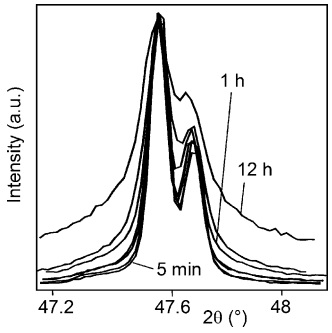

Fig. 7. 1 2 3 cubic X-ray diffraction peak ($Cu K\alpha_1 + K\alpha_2$) of ball-milled $La_{1.9}Y_{0.1}Mo_2O_9$ after various milling times.

3.2. Densification of ball-milled samples

As described in the next section, the attrition treatment introduces a contamination by zirconia in the powders. To avoid this problem, planetary ball milling using agate balls and jars was tested to reduce the particle size. Several preliminary tests have been carried out on the compound $La_{1.9}Y_{0.1}Mo_2O_9$. For each test, one pellet has been shaped by uniaxial pressure in a 10 mm steel matrix, and then pressed at 350 MPa in a water isostatic press. Initial powders have been milled for various periods from 1 min to 24 h. The pellets were sintered in the same conditions for 24 h at 950 °C. This rigorous procedure ensures that the particle size of powders is the only variable parameter to affect the densification of samples. Fig. 7 shows a scan of the cubic 123 reflexion collected by high resolution X-ray powder diffraction. Its full width at half maximum increases with increasing milling time, which indicates a reduction of the coherent diffraction domains, and therefore a reduction of the average grain size. All the powders are white before and after milling, for all milling times except for 24 h (96 × 15 min), for which the color is slightly greyish. It may result from a slight reduction of hexavalent molybdenum (and consecutive oxygen loss), rather than from pollution (see below). For milling times ranging from 1 min to 24 h, no deterioration of the compound has been evidenced by X-ray diffraction. Fig. 8 shows the evolution, versus milling time, of the relative density of the pellets after sintering. This relative density increases from 82 to 98% after 12 h of ball milling treatment (see Table 2). A 96% relative density can be reached for only two 15 min sequences (separated by a 15 min pause sequence). However, it is necessary to mill 25 times longer to reach 98% of relative density. The densification of the samples is confirmed by the SEM micrographs of the polished-faces of $La_{1.9}Y_{0.1}Mo_2O_9$ pellets presented in Fig. 9. The microstructure is fully dense for the sample prepared from powders issued from 12 h milling.

Table 2
Evolution of the absolute and relative densities of different samples with composition $La_{1.9}Y_{0.1}Mo_2O_9$ upon ball milling time[a]

Milling time (min)	Density (g cm^{-3})	Relative density (%)[a]
0	4.526	81.8
5	4.839	87.5
10	4.936	89.2
15	5.121	92.6
30	5.271	95.3
60	5.311	96
720	5.4	97.7
1440	5.4	97.7

[a] Theoretical density = 5.53 g cm^{-3}.

Thus, for an average grain size lower than 1 μm, the densification of the samples is possible by adjusting the sintering conditions for each composition.

These grinding conditions were applied to all the studied compounds. The sintering temperatures were the same as that determined for samples issued from attrition milling. The final reached relative density was also around 96%.

3.3. Electrical resistivity stability as a function of time

During the impedance measurements on pellets prepared from attrited powders, we noticed, at a given constant temperature, an abnormal drift of total electrical resistivity with time. As an illustration, the resistance measured at 585 °C

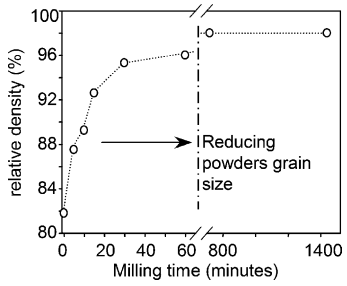

Fig. 8. Relative density of $La_{1.9}Y_{0.1}Mo_2O_9$ pellets sintered at 950 °C as a function of the initial powder milling time.

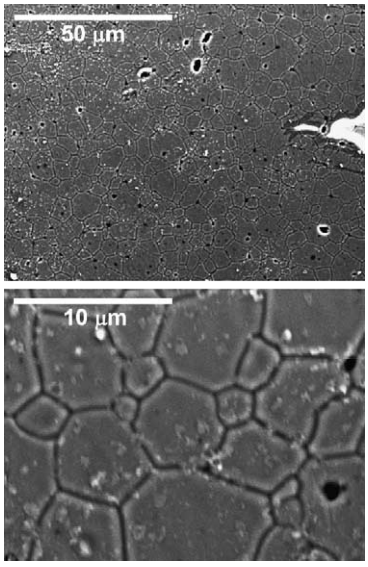

Fig. 9. SEM micrographs of sintered $La_{1.9}Y_{0.1}Mo_2O_9$ pellet, prepared from ball-milled powders during 12 h.

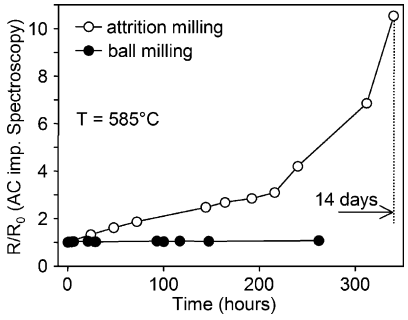

Fig. 10. Evolution as a function of time of the measured resistance (R/R_0) of two $La_{1.7}Gd_{0.3}Mo_{0.8}W_{1.2}O_9$ pellets at $T = 585\,^{\circ}C$, one issued from ball-milled powders (black circles), the other from attrited powders (open circles).

on a $La_{1.7}Gd_{0.3}Mo_{0.8}W_{1.2}O_9$ pellet (relative density around 96%) is presented in Fig. 10 (open circles): it shows a significant augmentation with time.

The same type of measurement at 585 °C has been carried out on pellets issued from ball-milled powders, on a comparable sample (composition, dimensions, ceramic treatments, relative density). It did not show any evolution of the measured resistance (Fig. 10, black circles). We have therefore tried to detect, in the powders and pellets, an eventual pollution from the elements present in each milling apparatus (Zr for attrition and Si for ball milling).

Energy dispersive X-ray spectroscopy experiments have been carried out in both cases. Fig. 11 presents the EDX spectra collected on $La_{1.9}Y_{0.1}Mo_2O_9$ ball-milled powders (for different milling durations), and on $La_{1.7}Gd_{0.3}Mo_2O_9$ and $La_{1.7}Gd_{0.3}Mo_{0.8}W_{1.2}O_9$ attrited powders (for 3 h). In the ball milling case, no trace of silicium has been detected at its Kα energy peak, whatever the milling time. On the contrary, in the attrition case (Fig. 11b) the zirconium Kα peak is detected for all compositions. We can thus evidence that some pollution has been introduced by the zirconia balls, which strongly affects the transport properties.

Furthermore, the X-ray diffractogram of a pellet issued from attrition milling after the resistivity measurement indicates the formation of an extra phase through the appearance of a small diffraction peak. This reflexion alone is too small to identify unambiguously the compound, but it is very close to the strongest diffraction peak of insulating pyrochlore-type phase $La_2Zr_2O_7$. It is likely that such an impurity phase forms progressively at grain boundaries, leading

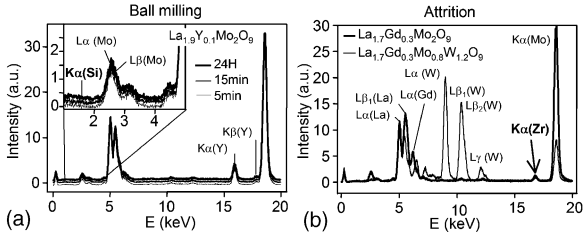

Fig. 11. EDX spectra of LAMOX powders: (a) ball-milled $La_{1.9}Y_{0.1}Mo_2O_9$ after different milling times; (b) attrited $La_{1.7}Gd_{0.3}Mo_2O_9$ and $La_{1.7}Gd_{0.3}Mo_{0.8}W_{1.2}O_9$.

to an increasingly insulating sample. This problem has already been observed at yttria-stabilized zirconia–lanthanum perovskites interfaces. No extra diffraction peak is observed in the ball-milled samples, indicating that a potential weak Si contamination, if any, would remain spread over the LAMOX phase with no detectible incidence on the transport properties.

The above observations incited us to set aside the pellets prepared by attrition milling and use those prepared by ball milling for the conductivity measurements presented in the next section.

3.4. Charge transport versus porosity

The effects of pores on the samples electrical properties have been characterized. Indeed, it is now well demonstrated that ceramics microstructure could have a strong effect on the electrical properties.[15–24] The impedance spectra at 375 °C of six samples, originating from ball-milled powders and with different relative densities ranging from 81.8 to 98% (see some micrographs on Fig. 12), are presented in Fig. 13. The electrical responses recorded into wet atmospheric air and into dried nitrogen are identical. In most cases, only one well-defined semicircle is observed at high frequency. In contrast to observation in YSZ ionic oxygen conductor[16–19] the presence of pores does not result in a separate semicircle. No additional blocking effect could be evidenced at lower frequencies, except for the denser samples, for which a small additional semicircle appears. The latter probably corresponds to a grain boundaries blocking effect.[17] This small effect of grain boundaries in comparison with the main effect related to porosity will not be taken into account here.

Impedance diagrams of all samples were fitted with only one semicircle (high frequencies domain) using an equivalent electrical circuit composed of a resistor R, connected in parallel with a constant phase element, CPE. The CPE contribution is an empirical impedance function of the type:

$$Z(\omega)_{\mathrm{CPE}} = \frac{1}{C(j\omega)^p}; \qquad (-1 \le p \le 1)$$

The phase angle γ is given by $\gamma = p\pi/2$. Each curve has been fitted with a single parallel R//CPE model by a least squares

Table 3
High frequency semicircles characteristics (resistivity, relaxation frequency, equivalent capacity and phase angle) of the $La_{1.9}Y_{0.1}Mo_2O_9$ impedance spectra measured at 375 °C on pellets with different relative density

Compacity (%)	R ($\times 10^5\ \Omega$ cm)	ω_0 ($\times 10^5$ rad s^{-1})	$\mathrm{CPE}_{\mathrm{eq}}$ ($\times 10^{-11}$ F)	γ (°)
81.8	2.848	6	3.07	7.44
87.5	2.483	6.55	3.07	6.53
89.3	2.380	6.57	3.22	6.83
92.6	2.166	7.24	4.27	7.88
95.3	1.940	8.18	3.96	7.8
98	1.912	6.55	3.65	6.6

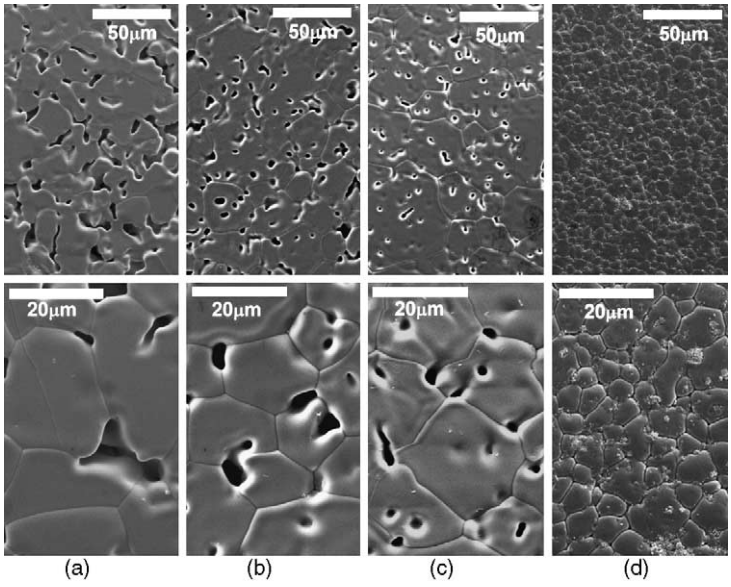

Fig. 12. SEM micrographs of sintered $La_{1.9}Y_{0.1}Mo_2O_9$ pellets with different relative densities: (a) 81.8%, (b) 87.5%, (c) 92.6%, (d) 98%.

refinement. The fit parameters of the high frequency semicircle are summarized in Table 3 for all samples. The differences in sample resistance R (semicircle diameter), attributed to the presence of the pores, are consistent with the expectation that electrical resistivity of a material increases with increasing porosity. The Arrhenius conductivity plots of four samples with different relative densities, which have been carefully collected within the (300–400 °C) temperature range, are presented on Fig. 14. The samples conductivity is improved by increasing their relative density (lowering the pore fraction volume). Moreover, the higher the relative density and the conductivity, the lower the curve slope.

This last remark indicates that the conductivity of all the samples should join at high temperature, the effect of microstructure defects being thus lowered by temperature. Such a phenomenon has already been reported.[17,18] The change in curve slope is significant of a change in the conduction mechanism.

Fig. 15 presents the evolution of the measured resistance of the ceramic samples with increasing porosity. The resistance increase, called $\Delta R/R_0$ and expressed in %, seems to evolve linearly with porosity within the studied range, according to the relationship $\Delta R/R_0 = 3.4 \times$ (porosity). For instance, a porosity around 20 vol% lowers the total conductivity to about 60% of that of the pure bulk material (≅single crystal).

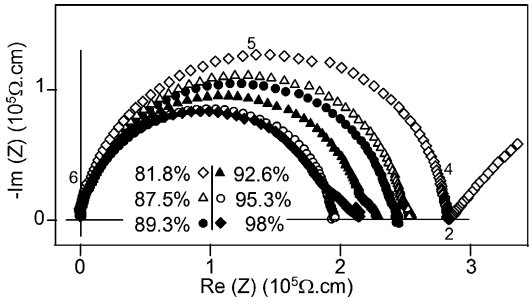

Fig. 13. Impedance spectra recorded at 375 °C on $La_{1.9}Y_{0.1}Mo_2O_9$ samples with different relative densities. For clarity, the electrode polarization and log (measured frequency) are shown for the sample with 81.8% relative density only.

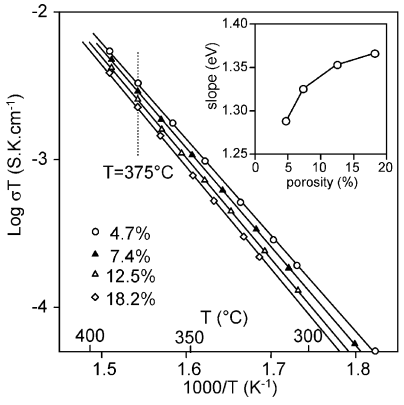

Fig. 14. Arrhenius plots of conductivity for $La_{1.9}Y_{0.1}Mo_2O_9$ samples with various volumic porosities (18.2–4.7%). In the insert: evolution of the curves slope with porosity.

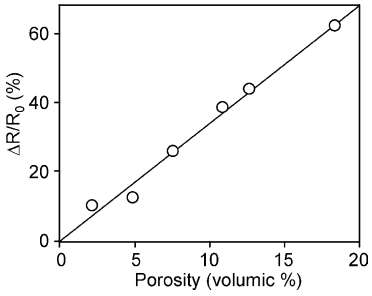

Fig. 15. Resistance at 375 °C as a function of porosity for a series of pellets with composition $La_{1.9}Y_{0.1}Mo_2O_9$.

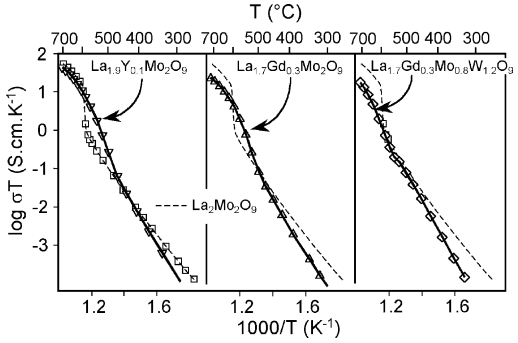

Fig. 16. Electrical conductivity of parent compound $La_2Mo_2O_9$, and substituted $La_{1.9}Y_{0.1}Mo_2O_9$, $La_{1.7}Gd_{0.3}Mo_2O_9$ and $La_{1.7}Gd_{0.3}Mo_{0.8}W_{1.2}O_9$.

3.5. Charge transport versus composition in dense samples

The conductivity of the optimized compositions was measured using ac impedance spectroscopy on the densified samples (ball milling case, relative density >96%). These compounds can be considered as pure ionic conductors, the electronic transference number of $La_2Mo_2O_9$ being equal to 10^{-3} at 750 °C.[25,26]

The result of the electrical measurements is presented in Fig. 16 for $La_2Mo_2O_9$, $La_{1.9}Y_{0.1}Mo_2O_9$, $La_{1.7}Gd_{0.3}Mo_2O_9$, and $La_{1.7}Gd_{0.3}Mo_{0.8}W_{1.2}O_9$. The disappearance of the conductivity jump at around 580 °C confirms the chemical stabilization of the cubic form at room temperature, as mentioned elsewhere.[6,7] In spite of the suppression of the phase transition, the conductivity curves do not exhibit an Arrhenius behavior in the whole thermal range. A first interpretation of this behavior was reported elsewhere.[26] When compared to $La_2Mo_2O_9$, a strong increase of the ionic mobility activation energy at low temperature is observed in substituted compounds (Fig. 13). Above 600 °C, one can notice that all the substituted compounds have lower conductivities than the parent compound. In a previous paper,[7] we have reported that rare earths substitutions in $La_2Mo_2O_9$ seem to increase the ionic conductivity (measurements with non-optimized microstructures), but pointed out a strong correlation between the measured σ values and the relative densities of the corresponding samples. We can now understand that it resulted mainly from the microstructure effects in porous samples. As the chemical composition strongly affects the sintering behavior (Fig. 5), applying the same annealing conditions to the different compositions led to samples with different relative densities, which strongly affects the ac impedance measurements.

Thus, after rigourous measurements on dense samples, an important result is that all the substituted compounds studied here present at high temperature a lower conductivity than the parent compound $La_2Mo_2O_9$. The latter remains above 600 °C the best member of the LAMOX family with respect to ionic conductivity. Just below the structural transition however, i.e. around 500–550 °C, substitution can increase the ionic conductivity due to stabilization of the cubic phase.

4. Conclusion

From the two methods used here to lower grain sizes of LAMOX materials in order to get dense sintered samples, only ball milling could be retained because of a pollution problem by zirconia in attrition milling. Densification of selected LAMOX compounds appeared to be easy after a careful dilatometric study. Proper milling procedures in agate jars with a planetary milling apparatus, followed by appropriate sintering, allow the control of the ceramics relative density.

We have shown in a previous study[7] that the electrical properties appear to be closely related to compacity, which points out the importance of its control. It has been confirmed by the present work, which depicts the incidence of porosity on the ionic transport. A thorough study of the optimal sintering conditions is absolutely necessary before any determination of the incidence of chemical substitution on the transport properties. Interestingly enough, the stabilization of $La_2Mo_2O_9$ against reduction by tungsten substitution[8] is not too detrimental to oxide ion conduction, which is an interesting result in view of applications as electrolyte in SOFC.

Not so surprisingly, isovalent substitutions in general do not affect significantly (apart from the suppression of the phase/conducting transition) the magnitude of ionic transport. The latter however is expected to be more affected by aliovalent substitutions.

Acknowledgements

The authors are grateful to ADEME (French Environment and Energy Agency) and Rhodia Electronics & Catalysis for their grant and financial supports. They express their thanks to Dr. O. Bohnke for her contribution to complex impedance spectroscopy measurements.

References

1. Fournier, J. P., Fournier, J. and Kohlmuller, R., Etude des systèmes $La_2O_3-MoO_3$, $Y_2O_3-MoO_3$ et des phases Ln_6MoO_{12}. *Bull. Soc. Chim. Fr.*, 1970, 4277–4283.
2. Lacorre, P., Goutenoire, F., Bohnke, O., Retoux, R. and Laligant, Y., Designing fast oxide-ion conductors based on $La_2Mo_2O_9$. *Nature*, 2000, **404**, 856–858.
3. Goutenoire, F., Isnard, O., Retoux, R. and Lacorre, P., On the crystal structure of $La_2Mo_2O_9$, a new fast oxide-ion conductor. *Chem. Mater.*, 2000, **12**, 2575–2580.
4. Goutenoire, F., Isnard, O., Suard, E., Bohnke, O., Laligant, Y., Retoux, R. *et al.*, Structural and transport characteristics of the LAMOX family of fast oxide-ion conductors, based on lanthanum molybdenum oxide $La_2Mo_2O_9$. *J. Mater. Chem.*, 2001, **11**, 119–124.
5. Arulraj, A., Goutenoire, F., Tabellout, M., Bohnke, O. and Lacorre, P., Synthesis and characterization of the anionic conductor

system $La_2Mo_2O_{9-0.5x}F_x$ ($x = 0.02$–0.30). *Chem. Mater.*, 2002, **14**, 2492–2498.
6. Georges, S., Goutenoire, F., Laligant, Y. and Lacorre, P., Improving oxide-ion conduction in the LAMOX family. In *Proceedings of the 5th European SOFC Forum, Vol 2*, 2002, pp. 671–678.
7. Georges, S., Goutenoire, F., Altorfer, F., Sheptyakov, D., Fauth, F., Suard, E. *et al.*, Thermal, structural and transport properties of the fast oxide-ion conductors $La_{2-x}R_xMo_2O_9$ (R = Nd, Gd, Y). *Solid State Ionics*, 2003, **161**, 231–241.
8. Georges, S., Goutenoire, F., Laligant, Y. and Lacorre, P., Reducibility of fast oxide-ion conductors $La_{2-x}R_xMo_{2-y}W_yO_9$ (R = Nd, Gd). *J. Mater. Chem.*, 2003, **13**, 2317–2321.
9. Collado, J. A., Aranda, M. A. G., Cabeza, A., Olivera-Pastor, P. and Bruque, S., Synthesis, structures, and thermal expansion of the $La_2W_{2-x}Mo_xO_9$ series. *J. Solid State Chem.*, 2002, **167**, 80–85.
10. Boivin, J. C. and Mairesse, G., Recent material developments in fast oxide ion conductors. *Chem. Mater.*, 1998, **10**, 2870–2888.
11. Subasri, R., Matusch, D., Nafe, H. and Aldinger, F., Synthesis and characterization of $(La_{1-x}M_x)_2Mo_2O_{9-\delta}$; M = Ca^{2+}, Sr^{2+} or Ba^{2+}. *J. Eur. Ceram. Soc.*, 2004, **24**, 129–137.
12. Marrero-Lopez, D., Ruiz-Morales, J. C., Nunez, P., Abrantes, J. C. C. and Frade, J. R., Synthesis and characterization of $La_2Mo_2O_9$ obtained from freeze-dried precursors. *J. Solid State Chem.*, 2004, **177**, 2378–2386.
13. Marozau, I. P., Marrero-López, D., Shaula, A. L., Kharton, V. V., Tsipis, E. V., Núñez, P. *et al.*, Ionic and electronic transport in stabilized β-$La_2Mo_2O_9$ electrolytes. *Electrochim. Acta*, 2004, **49**, 3517–3524.
14. Lacorre, P. and Retoux, R., First direct synthesis by high energy ball milling of a new lanthanum molybdate. *J. Solid State Chem.*, 1997, **132**, 443–446.
15. Wang, D. Y. and Nowick, A. S., The grain-boundary effect in doped ceria solid electrolytes. *J. Solid State Chem.*, 1980, **35**, 325–333.
16. Steil, M. C., Thevenot, F. and Kleitz, M., Densification of yttria-stabilized zirconia. Impedance spectroscopy analysis. *J. Electrochem. Soc.*, 1997, **144**, 390–398.
17. Kleitz, M., Dessemond, L. and Steil, M. C., Model for ion-blocking at internal interfaces in zirconias. *Solid State Ionics*, 1995, **75**, 107–115.
18. Kleitz, M., Dessemond, L., Steil, M. C. and Thevenot, F., Correlations between medium frequency blocking parameters and microstructure in low-conductivity materials. In *Proceedings of the Materials Research Society Symposium (Electrically Based Microstructural Characterization), Vol 411*, 1996, pp. 269–275.
19. Ciacchi, F. T., Crane, K. M. and Badwal, S. P. S., Evaluation of commercial zirconia powders for solid oxide fuel cells. *Solid State Ionics*, 1994, **73**, 49–61.
20. Benkaddour, M., Conflant, P., Drache, M. and Steil, M. C., Evolution of microstructure and impedance upon the sintering of a Bi–Pr–V-based fluorite-type oxide conductor. *Solid State Ionics*, 2002, **146**, 175–184.
21. Kleitz, M. and Steil, M. C., Microstructure blocking effects versus effective medium theories in YSZ. *J. Eur. Ceram. Soc.*, 1997, **17**, 819–829.
22. Badwal, S. P. S., Grain boundary resistivity in zirconia-based materials: effect of sintering temperatures and impurities. *Solid State Ionics*, 1995, **76**, 67–80.
23. Florio, D. Z. and Muccillo, R., Sintering of zirconia-yttria ceramic studied by impedance spectroscopy. *Solid State Ionics*, 1999, **123**, 301–305.
24. Lee, J.-H., Mori, T., Li, J.-G., Ikegami, T. and Takenouchi, S., Impedance spectroscopic estimation of inter-granular phase distribution in 15 mol% calcia-stabilized zirconia/alumina composites. *J. Eur. Ceram. Soc.*, 2001, **21**, 13–17.
25. Georges, S., Skinner, S. J., Lacorre, P. and Steil, M. C., Oxide ion diffusion in optimised LAMOX materials. *J. Chem. Soc., Dalton Trans.*, 2004, 3101–3105.
26. Georges, S., Goutenoire, F., Bohnke, O., Steil, M. C., Wiemhöfer, H. D. and Lacorre, P., The LAMOX family of fast oxide-ion conductors: overview and recent results. *J. New. Mater. Electrochem. Syst.*, 2004, **7**, 51–57.